Viser Technology Pte. Ltd.
Research and Application of Materials Science
DOI: 10.33142/rams.v5i2.12704

Research Article Open Access

Improved Corrosion Behavior of Biodegradable Mg-4Zn-1Mn Alloy Modified by Sr/F co-doped CaP Micro-arc Oxidation Coatings

Weirong LI[1*], Yanfang LI [1], Qian LI [1], Xuan XIONG[1], Fangfei LIU[1], Ronghui LI [1], Heng LI[1], Dong PANG[1], Jia LU[2], Xuan ZHANG [2*]

1. Dongguan Eontec Co., Ltd., Dongguan, Guangdong, 523000, China
2. School of Mechanical Engineering, Tiangong University, Tianjin 300387, China

[*] ***Corresponding Author:*** *Weirong LI, Xuan ZHANG, E-mail: liwr@e-ande.com; zhangxuan199706@163.com*

Abstract

The Sr/F co-doped CaP (Sr/F-CaP) coatings were prepared by micro-arc oxidation (MAO) under different voltages to modify the microstructure and corrosion behavior of Mg-4Zn-1Mn alloy. The surface and interface characteristics investigated using scanning electron microscopy (SEM) and energy dispersive X-ray spectrometer (EDS) showed that the MAO coatings displayed uneven crater-like holes and tiny cracks under lower voltage, while they exhibited relatively homogeneous crater-like holes without cracks under higher voltage. The thickness of MAO coatings increased with increasing voltage. The corrosion behavior of Mg-4Zn-1Mn alloy was improved by the MAO coatings. The MAO coatings prepared under 450 V and 500 V voltages possessed the best corrosion resistance with regard to the electrochemical corrosion tests and immersion corrosion tests, respectively. The MAO coatings fabricated under 450-500 V could provide a better corrosion protection effect for the substrate.

Keywords: *Biodegradable Mg alloys; Mg-4Zn-1Mn alloy; Micro-arc oxidation; Sr/F co-doped CaP coatings*

1 Introduction

As a representative kind of biodegradable metals, Mg alloys have recently attracted great research interest as temporary implants in the orthopedic and cardiovascular fields [1-2]. Compared with traditional biomedical metals (stainless steels, Ti alloys, NiTi alloys and Co-Cr alloys, etc.), Mg alloys exhibit the following advantages[3-5]: Firstly, they have lower density, higher specific strength and closer Young's modulus to that of human bone; Secondly, they can be gradually dissolved in physiological environment after tissue repairing to avoid a secondary removal surgery; Thirdly, their corrosion products of Mg oxides/hydroxides are nontoxic and may even promote cell viability. However, the insufficient mechanical support and excess hydrogen accumulation caused by the rapid corrosion of Mg alloys usually hinder the tissue repairing process in early implantation period, which is the main obstacle for their clinical applications [6-7]. Therefore, enhancing the corrosion resistance of Mg alloys is the key means to solve their clinical problems.

Surface modification via proper technologies such as ion implantation, magnetron sputtering, anodic oxidation, electrochemical deposition, sol-gel and spin coating has been evidenced to be an effective method to improve the corrosion behavior of Mg alloys [8-13]. Among them, the micro-arc oxidation (MAO) is a very promising surface modification method for Mg alloys, which can regulate their corrosion behavior by preparing corrosion-resistant ceramic coatings with desired microstructure, morphology and chemical composition [14-17]. Generally, the MAO coatings exhibit a bilayer feature: the outer layer with porous microstructure contributes to promote the adhesion, migration and growth of cells; the inner layer with dense microstructure helps to enhance the corrosion resistance of outer layer and increase its bonding strength with the substrate [18]. The major factors influencing MAO coatings are electrolyte composition and electrical parameters including working mode, voltage, current density, oxidation time, frequency, duty ratio, etc. Ly et al. compared the effect of different working modes (unipolar, bipolar, unipolar followed by bipolar) on the corrosion resistance of MAO coatings on the Mg-4.71Zn-0.6Ca alloy surface, and found that the

Received on September 22, 2023; Accepted on November 2, 2023

MAO coating prepared under hybrid mode had better anti-corrosion ability than the other two modes[19]. Lin et al. fabricated the forsterite-containing MAO coatings on the surface of ZK60 Mg alloy via a silicate electrolyte-based MAO treatment under different voltages, and the results showed that the corrosion resistance of MAO coatings were increased with increasing voltage [20]. Zhu et al. further enhanced the corrosion resistance of molybdate conversion coating on the surface of AZ91D Mg alloy after a MAO treatment in the electrolyte with Na_2SiO_3 as main salt, and observed that the ceramic coating was gradually formed as the oxidation time was prolonged [21].

Considering that Ca and P elements are the main components of human bone, the CaP MAO coatings have been prepared to simultaneously improve the corrosion behavior and biocompatibility of Mg alloys [22-23]. However, the single CaP coatings lack adequate bioactivity like antibacterial and osteogenic properties, which can be compensated by doping some functional elements. As a necessary trace element for human body, Sr element can not only stimulate bone formation but also inhibit bacterial growth, which is an ideal element for bone regeneration [24]. As a participating element for multifarious metabolic activities, F element can facilitate osteoblasts differentiation to accelerate bone formation and provide broad-spectrum antibacterial property[25]. Therefore, the co-doping of Sr and F elements into the CaP coatings (Sr/F-CaP coatings) is expected to have satisfactory corrosion resistance and higher bioactivity with both antibacterial and osteogenic properties. To our knowledge, there are no systematic researches on the biodegradable Mg alloys modified by the Sr/F-CaP coatings. In this work, the effects of Sr/F-CaP coatings prepared by MAO under different voltages on the microstructure and corrosion behavior of extruded Mg-4Zn-1Mn alloy were investigated.

2 Experimental Procedures

2.1 Sample preparation

2.1.1 Substrate

The high-purity Mg (＞99.99%), high-purity Zn (＞99.99%) and Mg-5Mn intermediate alloy were used as the raw materials. The raw materials were melted using an electric resistance furnace protected by the mixed gas of 0.3 vol.% SF_6, 50 vol.% CO_2 and 49.7 vol.% air. The alloy melt was purged at 760 ℃ for 10 min, held at 720 ℃ for 15 min, poured into a mild steel crucible preheated at 700 ℃ and cooled at room temperature to get the Mg-4Zn-1Mn ingot (Φ100 mm×200 mm). After that, the ingot was machined to remove the oxides and impurities on the surface to get the initial rod with a diameter of 80 mm. For extrusion process, the initial rod was preheated at 450 ℃ and extruded at 380 ℃ with an extrusion rate of 1.5 mm/min and an extrusion ratio of 64 to obtain the Mg-4Zn-1Mn rod (Φ10 mm×1000 mm). Before MAO treatment, the rod was cut into Φ10 mm×3 mm sheets by the electro-discharge machining. The sheets (used as the substrates) were mechanically polished, ultrasonically cleaned with distilled water and dried in air.

2.1.2 MAO coatings

The MAO coatings were fabricated using a home-made MAO power supply under a constant voltage control mode. The samples and a stainless-steel plate with a size of 200 mm×200 mm×1 mm were served as the anode and the cathode, respectively. The electrolyte was composed of 15 g/L $Ca(H_2PO_4)_2·H_2O$, 15 g/L $Na_3PO_4·12H_2O$, 1.5 g/L CaF_2 and 2 g/L $Sr(OH)_2·8H_2O$. The electrolyte temperature was kept at 20-25 ℃ by a circulating water-cooling system. The samples and corresponding MAO processing parameters are listed in Table 1. After MAO process, the samples were rinsed with distilled water and dried in air.

Table 1 The samples and corresponding MAO processing parameters

Samples	Voltage (V)	Frequency (Hz)	Duty cycle (%)	Oxidation time (min)
Sr/F-CaP-400	400	600	30	8
Sr/F-CaP-450	450	600	30	8
Sr/F-CaP-500	500	600	30	8

2.2 Microstructure characterization

The surface and cross-sectional morphologies of the MAO coatings were analyzed by a scanning electron microscopy (SEM, Quanta-450, FEI, USA) and an energy dispersive X-ray spectrometer (EDS, Oxford Instruments, UK). The phase constitutions of the MAO coatings were identified by an X-ray diffractometer (XRD, D8 Advance, Bruker, Germany) with a Cu K_α radiation at a scanning rate of 4^o/min in the 2θ range of 10^o～85^o.

2.3 Corrosion behavior evaluation

2.3.1 Electrochemical corrosion tests

The electrochemical corrosion behavior of the samples before and after MAO treatment was studied at an electrochemical workstation (CHI660e, CH Instruments Inc., China). A typical three-electrode system was employed with the samples as the working electrode, a platinum electrode as the counter electrode and a saturated calomel electrode (SCE) as the reference electrode. The measurements were performed in the simulated body fluid (SBF) at 37±1 ^{o}C. The composition of the SBF included 8.035 g/L NaCl, 0.355 g/L $NaHCO_3$, 0.225 g/L KCl, 0.231 g/L $KH_2PO_4·3H_2O$, 0.311 g/L $MgCl_2·6H_2O$, 39 mL HCl (1.0M), 0.292 g/L $CaCl_2$, 0.072 g/L Na_2SO_4 and 6.118 g/L Tris[26]. The electrochemical corrosion tests of open circuit potential (OCP),

impedance spectroscopy (EIS) and potentiodynamic polarization (PDP) were conducted in sequence. The OCP values were recorded for 30 min to realize surface stabilization. The EIS results were measured with an AC amplitude perturbing signal of 5 mV and a scan frequency from 100 kHz to 10 mHz. The EIS data were fitted by the ZSimpWin software. The PDP curves were tested at a scan rate of 1 mV/s with a potential range from -2 V/SCE to -1 V/SCE. The PDP data were fitted by the CHI660e software.

2.3.2 Immersion corrosion tests

The immersion corrosion behavior of the samples before and after MAO treatment was investigated in the SBF at 37 ±1 °C according to the ASTM-G31-72 standard. After different immersion times (2, 6 and 14 days), the samples were taken out, rinsed with distilled water and dried in air. The morphology and composition of the corrosion products at specific immersion time were analyzed by the SEM and EDS. The pH value of SBF during immersion corrosion tests was monitored by a pH meter (PHB-4, INESA Scientific Instrument, Shanghai, China). The weight loss of the samples was measured by a scale (0.01 mg in accuracy) after removing the corrosion products with the chromic acid solution (200 g/L CrO_3 and 10 g/L $AgNO_3$).

3 Results and Discussion

3.1 Microstructure

Figure 1 shows the surface and the cross-section morphologies of the samples. The substrate surface is relatively smooth and flat, which is convenient for the subsequent coating process (Figure 1a). The Sr/F-CaP-400 sample surface is characterized by uneven crater-like holes and tiny cracks, whose average thickness of its MAO coating is about 7.8 μm (Figure 1b and 1e). There appears a transverse crack in the MAO coating of the Sr/F-CaP-400 sample, which may be caused by relatively low voltage of 400 V under a short oxidation time of 8 min. The growth rate of MAO coating is too small to prepare a thick-enough and high-quality coating under low voltage, which leads to the formation of a crack perpendicular to the growth direction. This can be evidenced by its unfavorable surface morphology and smallest average thickness, as shown in Figure 1b and 1e. The Sr/F-CaP-450 sample surface exhibits a compact morphology with homogeneous crater-like holes and its MAO coating has an average thickness of 9.2 μm (Figure 1c and 1f). The Sr/F-CaP-500 sample surface is featured with a dense morphology with various crater-like holes and its MAO coating has an average thickness of 11.0 μm (Figure 1d and 1g). The porous structure on the surface is generated due to the sparks discharge effect occurs in the MAO process, which could facilitate the cell growth in some degree [27]. The bonding interface between substrate and MAO coating becomes tighter as the voltage increases. With increasing voltage, the MAO coating shows a slightly larger thickness with relatively uniform porous structure and inconspicuous cracks. Similar phenomenon can also be found in the reference[28].

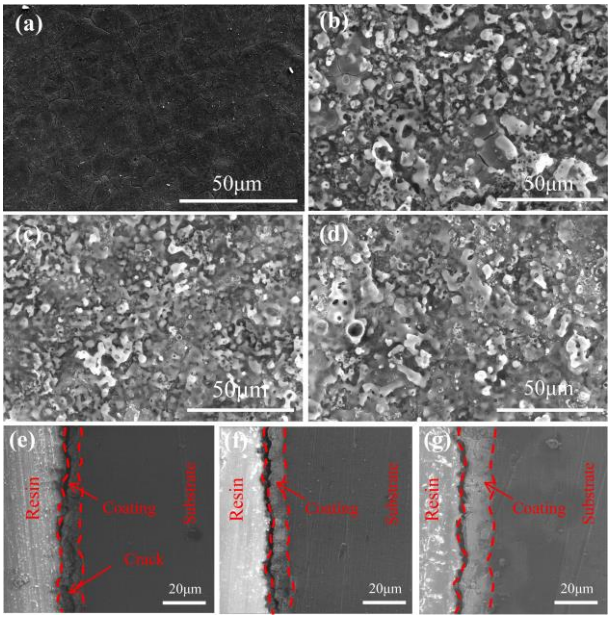

Figure 1 (a-d) surface and (e-g) cross-section morphologies of the samples: (a) substrate, (b, e) Sr/F-CaP-400, (c, f) Sr/F-CaP-450, (d, g) Sr/F-CaP-500

The chemical compositions of the samples are summarized in Table 2. The substrate is composed of 97.45 Mg, 2.03 Zn and 0.52 Mn (in at.%), whose chemical composition is close to the Mg-4Zn-1Mn alloy. For the MAO coatings, their chemical compositions include O, Mg, P major elements and Na, F, Ca, Zn, Ca, Sr minor elements, indicating that the Sr/F containing CaP coatings are deposited on the substrate surface.

Table 2 Chemical compositions of the samples (in at.%)

Samples	Mg	Zn	Mn	O	Sr	F	Ca	P	Na
Substrate	97.45	2.03	0.52	—	—	—	—	—	—
Sr/F-CaP-400	24.00	0.58	—	60.39	0.15	1.41	0.31	10.99	2.17
Sr/F-CaP-450	23.99	0.31	—	59.74	0.13	1.20	0.17	12.13	2.33
Sr/F-CaP-500	22.71	0.21	—	61.13	0.15	1.08	0.29	12.49	1.94

3.2 Corrosion behavior

Figure 2 demonstrates the EIS results of the samples in SBF at 37 °C. As shown in Figure 2a, the Nyquist plots of the samples consist of two parts: a capacitive reactance arc in the high-frequency region and an inductive reactance arc in the low-frequency region. Usually, a larger arc implies a higher anti-corrosion ability [29-30]. The MAO coatings exhibit larger capacitive reactance arc and inductive reactance arc than those of the substrate, suggesting that the former samples possess better corrosion resistance. The equivalent circuit for the

Nyquist plots is shown in Figure 2b and the fitting data are listed in Table 3. Here, the R_s is the solution resistance. The CPE_1 and CPE_2 represent the capacitive response of the corrosion products layer and the capacitance value at the solution/substrate interface, respectively. The R_1 and R_2 refer to the resistance of corrosion products layer (outer layer) and the charge transfer resistance (inner layer), respectively. It is noted that the samples have a higher R_2 value and a lower R_1 value, which demonstrates that the inner layer has a greater effect on the corrosion resistance than the outer layer. A similar result can also be found in the reference[31]. The R_p (R_1+R_2) can be used to evaluate the corrosion resistance of the samples, which increases in the order of substrate (511.0 Ω cm^2) < Sr/F-CaP-400 (2150.1 Ω cm^2) < Sr/F-CaP-500 (2887.3 Ω cm^2) ≈ Sr/F-CaP-450 (2830.3 Ω cm^2).

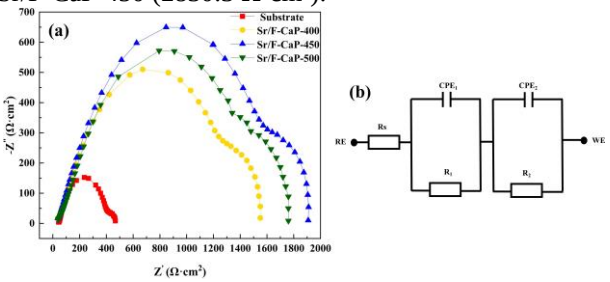

Figure 2 EIS results of the samples in SBF at 37 °C: (a) Nyquist plots, (b) equivalent circuit

Figure 3 presents the PDP curves of the samples in SBF at 37 °C. The electrochemical parameters fitted from the PDP curves are listed in Table 4. Generally, the E_{corr} represents the anti-corrosion ability of the coating and the i_{corr} indicates the corrosion rate once corrosion happens. A combination of larger E_{corr} and smaller i_{corr} usually stands for a better corrosion behavior[32]. The E_{corr} value of the substrate is about -1.570 V/SCE, while the E_{corr} value of the MAO coatings shows a slightly positive shift to -1.465 V/SCE, -1.502 V/SCE and -1.469 V/SCE for the Sr/F-CaP-400, Sr/F-CaP-400 and Sr/F-CaP-400 samples, respectively. Furthermore, the i_{corr} value increases in the order of Sr/F-CaP-450 (1.01×10^{-6} A cm^{-2}) ≈ Sr/F-CaP-400 (1.10×10^{-6} A cm^{-2}) < Sr/F-CaP-500 (1.94×10^{-6} A cm^{-2}) < < substrate (5.69×10^{-5} A cm^{-2}). This suggests that the MAO coatings can improve the corrosion behavior of Mg alloy to some extent. Similar results have been obtained by Shang et al [33].

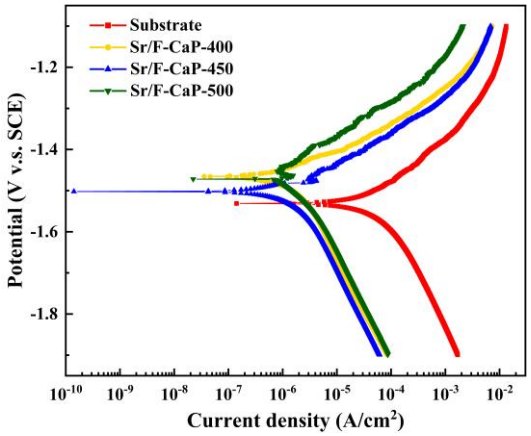

Figure 3 PDP curves of the samples in SBF at 37 °C

Table 4 Electrochemical parameters of corrosion potential (E_{corr}) and corrosion current density (i_{corr}) fitted from the PDP curves

Samples	E_{corr} (V/SCE)	i_{corr} (A cm^{-2})
Substrate	-1.570	5.69×10^{-5}
Sr/F-CaP-400	-1.465	1.10×10^{-6}
Sr/F-CaP-450	-1.502	1.01×10^{-6}
Sr/F-CaP-500	-1.469	1.94×10^{-6}

Figure 4 displays the corrosion morphologies of the samples after immersion in SBF at 37 °C for 2, 6, 14 days. After 2 days immersion, the substrate surface is obviously corroded to show lots of cracks (Figure 4a). From Figure 4b-4d, the surfaces of MAO coatings suffer varying degrees of corrosion. Comparatively, the corroded surfaces of MAO coatings remain relatively intact, which is evidenced from the compact morphology underneath the upper corrosion products layer. After 6 days immersion, the substrate surface is filled with deep corrosion cracks and variously sized corrosion fragments, which implies a corrosion tendency to the depth direction (Figure 4e). From Figure 4f-4h, the surfaces of MAO coatings exhibit a compact and uniform corrosion morphology. The corrosion cracks formed after 2 days immersion become less and smaller due to the deposition of corrosion products layer. It is noted that the surface of Sr/F-CaP-500 sample still remains some crater-like holes, suggesting that its MAO coating is not completely corroded during 6 days immersion. In addition, corrosion continues as the immersion time further increases to 14 days. The substrate surface is covered by randomly distributed

Table 3 Fitting data of the EIS results

Samples	R_s (Ω·cm^2)	CPE_1 (Ω^{-1} cm^{-2} s^{-n})	n_1	R_1 (Ω·cm^2)	CPE_2 (Ω^{-1} cm^{-2} s^{-n})	n_2	R_2 (Ω cm^2)	R_p (Ω cm^2)
Substrate	45.36	2.35×10^{-5}	0.80	122.0	7.57×10^{-4}	0.77	389	511.0
Sr/F-CaP-400	34.90	2.01×10^{-5}	0.66	521.1	9.18×10^{-5}	0.99	1629	2150.1
Sr/F-CaP-450	34.76	1.22×10^{-5}	0.68	890.3	5.63×10^{-5}	0.80	1997	2887.3
Sr/F-CaP-500	41.11	2.65×10^{-5}	0.64	887.3	5.73×10^{-5}	0.84	1943	2830.3

irregular corrosion products (Figure 4i). From Figure 4j-4l, there exist many blocky corrosion products on the corroded surfaces of MAO coatings. The blocky corrosion products tend to form a protective layer under higher voltage, which could retard further corrosion for the substrate.

Figure 5 illustrates the changes in pH value of the SBF and weight loss/weight loss rate of the samples during immersion corrosion tests. As shown in Figure 5a, the pH value of SBF increases rapidly in initial immersion period and then increases slowly in subsequent immersion period for all the four samples. The final pH value of SBF increases in the order of Sr/F-CaP-500 (7.71) < Sr/F-CaP-450 (7.81) < Sr/F-CaP-400 (7.87) < substrate (8.12). This increase in pH value of SBF is owing to the solution alkalization. As reported in the reference [34], both corrosion of Mg ($Mg + 2H_2O = Mg(OH)_2 + H_2$) and hydration of MgO ($MgO + 2H_2O = Mg(OH)_2$) exist on the surface of Mg alloys immersed in the corrosive media of SBF. The above reactions release abundant OH^- into the solution, which leads to the increase in pH value of SBF. An obvious reduction in pH value of SBF is observed for the MAO coatings compared with the substrate sample, indicating that the corrosion rate of Mg alloy is mitigated after MAO treatment. As shown in Figure 5b, the weight loss of samples increases with increasing immersion time, suggesting that corrosion continues during the immersion duration. After 14 days immersion time, the average weight loss increases in the order of Sr/F-CaP-500 (10.06 mg/cm^2) < Sr/F-CaP-450 (11.72 mg/cm^2) ≈ Sr/F-CaP-400 (12.23 mg/cm^2) < substrate (17.45 mg/cm^2) and it is reduced by 57.65%, 67.16% and 70.09% in comparison with that of substrate. Moreover, the weight loss rate of samples has a descending tendency as the immersion time increases, implying that the corrosion products layer has some protective effect on the substrate. At the end of 14 days immersion time, the average weight loss rate increases in the order of Sr/F-CaP-500 (0.72 $mg/cm^2/day$) < Sr/F-CaP-450 (0.84 $mg/cm^2/day$) ≈ Sr/F-CaP-400 (0.87 $mg/cm^2/day$) < substrate (1.25 $mg/cm^2/day$).

Figure 6 shows the SEM-EDS analysis of the corrosion products on the surface of substrate and Sr/F-CaP-500 samples after immersion in SBF for 14 days. The Sr/F-CaP-500 sample with the lowest corrosion rate is selected to investigate the corrosion products with the substrate sample being the control. In Figure 6a, the corrosion products on the surface of substrate exhibits coarse granular shape, whose composition is composed of 49.89 O, 1.67 Na, 8.04 Mg, 15.53 P, 23.06 Ca, 0.64 Mn and 1.17 Zn (in wt.%). In Figure 6b, the corrosion products on the surface of Sr/F-CaP-500 sample exhibits tiny acicular shape, whose composition is composed of 56.99 O, 34.79 Mg, 1.41 P and 6.82 Cl (in wt.%). The existence of MAO coating alters the formation process of corrosion products layer, which results in an improved corrosion behavior to some extent.

Figure 7 shows the schematic diagrams of possible corrosion mechanisms before and after MAO treatment. From Figure 7a, the substrate with a strong chemical activity easily reacts with H_2O in SBF to form $Mg(OH)_2$ and generate H_2. The $Mg(OH)_2$ is unstable and can react with corrosive ions like Cl^- to form soluble $MgCl_2$. After corrosion, there appear various corrosion pits on the surface. From Figure 7b, the MAO coatings can protect the substrate from corrosion in the initial corrosion period. As corrosion progresses, some random corrosion pits are formed on the MAO coatings, which gives a few passages for corrosive media and induces the corrosion of substrate. Because of the bilayer structure of MAO coatings (dense inner layer and porous outer layer), there tends to deposit more uniform and compact corrosion products layer on the surface. In summary, the MAO coatings can block the corrosive media from reaching the substrate and they also have good corrosion resistance, which retards the corrosion of substrate in the initial corrosion period.

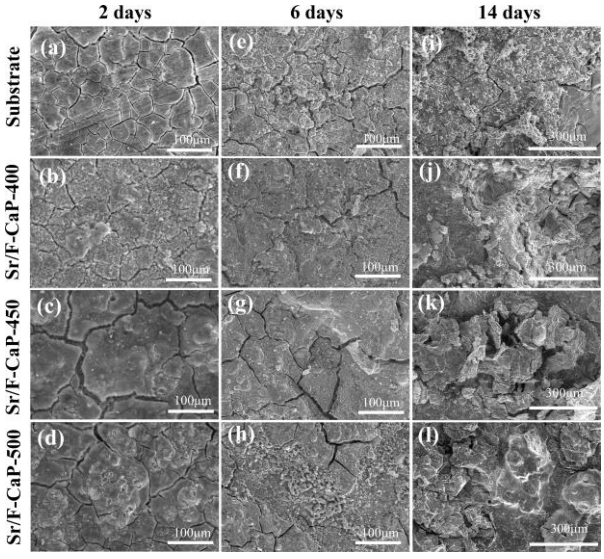

Figure 4 Corrosion morphologies of the samples after immersion in SBF at 37 °C for 2 days, 6 days and 14 days

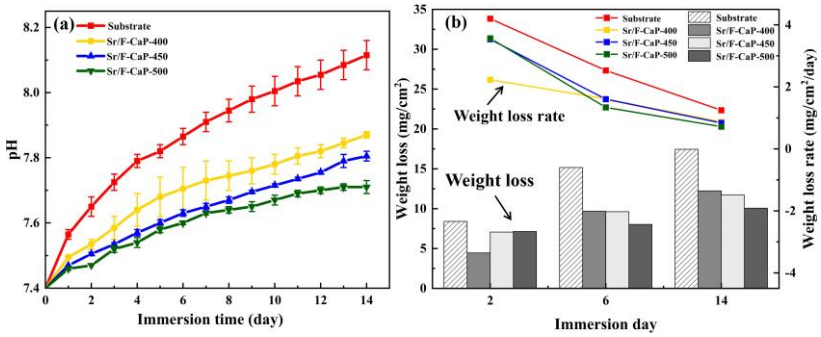

Figure 5 Changes in (a) pH value of the SBF, (b) weight loss/weight loss rate of the samples during immersion corrosion tests

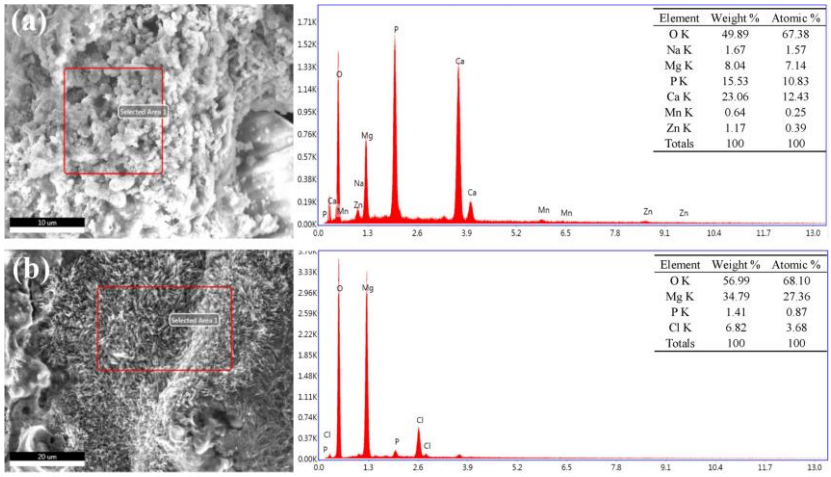

Figure 6 SEM-EDS analysis of the corrosion products on the surface of (a) substrate, (b) Sr/F-CaP-500 after immersion in SBF for 14 days

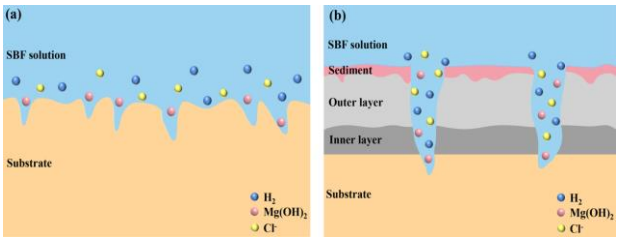

Figure 7 Schematic diagrams of possible corrosion mechanisms: (a) before and (b) after MAO treatment

It should be pointed out that there exists a certain disagreement in corrosion rate of the same sample between electrochemical corrosion result and immersion corrosion result. The best corrosion resistance is found for the Sr/F-CaP-450 sample and Sr/F-CaP-500 sample with respect to electrochemical corrosion tests and immersion corrosion tests, respectively. The reasons can be ascribed to the following two reasons: Firstly, the electrochemical corrosion tests are non-equilibrium and short-term corrosion evaluation method. Their results are mainly determined by the surface passivation that are affected by the cracks, holes, chemical compositions, etc. Secondly, the immersion corrosion tests are equilibrium and long-term corrosion evaluation method. Their results are influenced by the stability of corrosion products layer. Overall, the Sr/F-CaP MAO coatings fabricated under 450-500 V possess better corrosion resistance, which can provide the substrate a better protective effect.

4 Conclusion

The microstructure and corrosion behavior of Mg-4Zn-1Mn alloy surface modified by Sr/F-CaP MAO coatings have been studied. The main conclusions are as follows:

(1) The Sr/F-CaP MAO coatings bonded well with the Mg-4Zn-1Mn alloy. They exhibited uneven crater-like holes and tiny cracks under 400 V voltage and showed relatively homogeneous crater-like holes without cracks under 450 V and 500 V voltages. The thickness of MAO coatings increased from 7.8 μm to 11.0 μm as the voltage increased from 400 V to 500 V.

(2) The short-term corrosion behavior evaluated by electrochemical corrosion tests indicated that the MAO coatings could reduce the corrosion rate of substrate. The Sr/F-CaP-450 sample with the largest R_p value (2830.3 Ω cm^2) and smallest i_{corr} value (1.01×10^{-6} A cm^{-2}) had the lowest corrosion rate.

(3) The long-term corrosion behavior assessed by immersion corrosion tests demonstrated that the

corrosion resistance of substrate could be enhanced by the MAO coatings. The Sr/F-CaP-500 sample with the smallest weight loss (10.06 mg/cm^2) and weight loss rate (0.72 mg/cm^2/day) after 14 days immersion time exhibited the best corrosion resistance.

Author Contributions: Weirong Li: Investigation, Writing – review & editing. Yanfang Li: Investigation. Qian Li: Investigation. Xuan Xiong: Investigation. Fangfei Liu: Investigation. Ronghui Li: Investigation. Heng Li: Investigation. Dong Pang: Investigation. Jia Lu: Writing – review & editing. Xuan Zhang: Investigation, Writing – original draft.

Acknowledgements: This work did not receive any specific grant from funding agencies in the public, commercial, or not-for-profit sectors.

Declaration of Competing Interest: No potential conflicts of interest.

References

[1]Tsakiris V, Tardei C, Clicinschi F M. Biodegradable Mg alloys for orthopedic implants–A review[J]. Journal of Magnesium and Alloys, 2021, 9(6):1884-1905.

[2]Espiritu J, Meier M, Seitz J M. The current performance of biodegradable magnesium-based implants in magnetic resonance imaging: A review[J]. Bioactive Materials, 2021, 6(12):4360-4367.

[3]Song M S, Zeng R C, Ding Y F, et al.. Recent advances in biodegradation controls over Mg alloys for bone fracture management: A review[J]. Journal of materials science & technology, 2019, 35(4): 535-544.

[4]Liang J, Lei Z, Chen Y, et al.. Microstructure evolution of laser powder bed fusion ZK60 Mg alloy after different heat treatment[J]. Journal of Alloys and Compounds, 2022, 898: 163046.

[5]Ling L, Cai S, Li Q, et al.. Recent advances in hydrothermal modification of calcium phosphorus coating on magnesium alloy[J]. Journal of Magnesium and Alloys, 2022,10(1):62-80.

[6]Amukarimi S, Mozafari M. Biodegradable magnesium‐based biomaterials: An overview of challenges and opportunities[J]. MedComm, 2021,2(2):123-144.

[7]Zerankeshi M M, Alizadeh R, Gerashi E, et al.. Effects of heat treatment on the corrosion behavior and mechanical properties of biodegradable Mg alloys[J]. Journal of Magnesium and Alloys, 2022(21):78-82.

[8]Wei X, Liu P, Ma S, et al.. Improvement on corrosion resistance and biocompability of ZK60 magnesium alloy by carboxyl ion implantation[J]. Corrosion Science, 2020(173):108729.

[9]Yiu P, You J D, Wang S T, et al.. Tunable hydrophilicity in a surface nano-textured stainless steel thin film deposited by DC magnetron sputtering[J]. Applied Surface Science, 2021(555):149705.

[10]Jothi V, Adesina A Y, Kumar A M, et al.. Enhancing the biodegradability and surface protective performance of AZ31 Mg alloy using polypyrrole/gelatin composite coatings with anodized Mg surface[J]. Surface and Coatings Technology, 2020(381):125139.

[11]Rahman M, Li Y, Wen C. HA coating on Mg alloys for biomedical applications: A review[J]. Journal of Magnesium and Alloys, 2020,8(3):929-943.

[12]Li W, Su Y, Ma L, et al.. Sol-gel coating loaded with inhibitor on ZE21B Mg alloy for improving corrosion resistance and endothelialization aiming at potential cardiovascular application[J]. Colloids and Surfaces B: Biointerfaces, 2021(207): 111993.

[13]Wang T, Xu Y, Zhang Q, et al.. Enhancing the antibacterial properties of magnesium alloys with copper-doped anhydrous calcium phosphate nanoparticles embedded into the polycaprolactone coating for medical implants[J]. ACS Applied Nano Materials, 2022,5(12):18965-18976.

[14]Zhang K, Yu S. Preparation of wear and corrosion resistant micro-arc oxidation coating on 7N01 aluminum alloy[J]. Surface and Coatings Technology, 2020(388): 125453.

[15] Sankara Narayanan T S N , Il Song Park, Min Ho Lee. Strategies to improve the corrosion resistance of microarc oxidation (MAO) coated magnesium alloys for degradable implants: Prospects and challenges[J]. Progress in Materials Science, 2014, 60: 1.

[16]Xi K, Wu H, Zhou C, et al.. Improved corrosion and wear resistance of micro-arc oxidation coatings on the 2024 aluminum alloy by incorporation of quasi-two-dimensional sericite microplates[J]. Applied Surface Science, 2022(585):152693.

[17]Lin Z, Wang T, Yu X, et al.. Functionalization treatment of micro-arc oxidation coatings on magnesium alloys: A review[J]. Journal of Alloys and Compounds, 2021(879):160453.

[18]He R Y, Wang B Y, Xiang J H, et al.. Effect of copper additive on microstructure and anti-corrosion performance of black MAO films grown on AZ91 alloy and coloration mechanism[J]. Journal of Alloys and Compounds, 2021(889):161501.

[19]Ly X N, Yang S. Influence of current mode on microstructure and corrosion behavior of micro-arc oxidation (MAO) biodegradable Mg-Zn-Ca alloy in Hank's solution[J]. Surface and Coatings Technology, 2019(358):331-339.

[20]Lin Xiao, Tan Lili, Zhang Qiang, et al.. The in vitro degradation process and biocompatibility of a ZK60 magnesium alloy with a forsterite-containing micro-arc oxidation coating[J]. Acta Biomaterialia, 2019,9(10):8631–8642.

[21]Zhu H, Li X, Guan X, et al.. Effect of molybdate conversion coating of magnesium alloy reinforced by micro-arc oxidation[J]. Metals and Materials International, 2021(27):3975-3982.

[22]Chaharmahali R, Fattah-alhosseini A, Babaei K. Surface characterization and corrosion behavior of calcium phosphate (Ca-P) base composite layer on Mg and its alloys using plasma electrolytic oxidation (PEO): A review[J]. Journal of Magnesium and Alloys, 2021,9(1):21-40.

[23]Liu P, Wang J M, Yu X T, et al.. Corrosion resistance of bioinspired DNA-induced Ca–P coating on biodegradable magnesium alloy[J]. Journal of Magnesium and Alloys,

2019, 7(1): 144-154.
[24]Zhang Z Y, Huang T Y, Zhai D J, et al.. Study on strontium doped bioactive coatings on titanium alloys surfaces by micro-arc oxidation[J]. Surface and Coatings Technology, 2022(451):129045.
[25]Yu W, Sun R, Guo Z, et al.. Novel fluoridated hydroxyapatite/MAO composite coating on AZ31B magnesium alloy for biomedical application[J]. Applied Surface Science, 2019(464):708-715.
[26]Zheng Y, Zang L, Bi Y, et al.. Corrosion behavior of Fe/Zr composite coating on ZK60 Mg alloy by ion implantation and deposition[J]. Coatings, 2018,8(8):261.
[27]Küçükosman R, Şüküroğlu E E, Totik Y, et al.. Investigation of wear behavior of graphite additive composite coatings deposited by micro arc oxidation-hydrothermal treatment on AZ91 Mg alloy[J]. Surfaces and Interfaces, 2021(22): 100894.
[28]Yao J, Wang Y, Wu G, et al.. Growth characteristics and properties of micro-arc oxidation coating on SLM-produced TC4 alloy for biomedical applications[J]. Applied Surface Science, 2019(479):727-737.
[29]Jiang S, Zhang Z, Wang D, et al.. ZIF-8-based micro-arc oxidation composite coatings enhanced the corrosion resistance and superhydrophobicity of a Mg alloy[J]. Journal of Magnesium and Alloys, 2021(233):480-485.
[30]Xue K, Liang L X, Cheng S C, et al.. Corrosion resistance, antibacterial activity and drug release of ciprofloxacin-loaded micro-arc oxidation/silane coating on magnesium alloy AZ31[J]. Progress in Organic Coatings, 2021(158):106357.
[31]Kaseem M, Hussain T, Rehman Z U, et al.. Stabilization of AZ31 Mg alloy in sea water via dual incorporation of MgO and WO3 during micro-arc oxidation[J]. Journal of Alloys and Compounds, 2021(853):157036.
[32]H Wu Z, Shi X Zhang, A M Qasim, et al.. Achieving an acid resistant surface on magnesium alloy via bio-inspired design[J]. Applied Surface Science, 2019 (4789):150-161.
[33]Shang W, Wu F, Jiang S, et al.. Effect of hydrophobicity on the corrosion resistance of microarc oxidation/self-assembly/nickel composite coatings on magnesium alloys[J]. Journal of Molecular Liquids, 2021(330):115606.
[34]Xu W, Liu Z, Li B, et al.. Effects of magnetic field force in preparation of plasma electrolytic oxidation coatings: A novel method to improve the corrosion resistance of magnesium[J]. Journal of Alloys and Compounds, 2022(906):162642.